Microdynamic Study of Spin-Lattice Coupling Effects on Skyrmion Transport

Yifeng Wu,[1,2] Haohua Wen,[1,2,3,*] Weijin Chen,[1,2,4] and Yue Zheng[1,2,†]
[1]Centre for Physical Mechanics and Biophysics, School of Physics, Sun Yat-sen University, Guangzhou 510275, China
[2]State Key Laboratory of Optoelectronic Materials and Technologies, School of Physics, Sun Yat-sen University, Guangzhou 510275, China
[3]Sino-French Institute of Nuclear Engineering and Technology, Sun Yat-sen University, Zhuhai 519082, China
[4]School of Materials, Sun Yat-sen University, Shenzhen 518107, China

(Received 24 March 2021; revised 30 May 2021; accepted 27 July 2021; published 24 August 2021)

Skyrmion transport fundamentally determines the speed, energy consumption, and functionality of skyrmion-based spintronic devices, attracting considerable attention. Recent experimental studies found there is a migration barrier for the thermal activated transport of a skyrmion, which is speculated to be induced by the pinning effects of crystalline defects. In this Letter, we propose an alternative source of migration barrier for skyrmion transport, i.e., a local lattice distortion field due to spin-lattice coupling, which can lead to the same Arrhenius diffusion behavior in defect-free skyrmion materials. By performing spin-lattice dynamics simulations, we study the microdynamic insight into the influence of local lattice distortion field, which refreshes the mechanistic understanding on skyrmion transport.

DOI: 10.1103/PhysRevLett.127.097201

A skyrmion is a nanoscale magnetic structure in chiral magnetic materials [1–5]. As a topological stable structure, a skyrmion can be driven by a low electric current, which is thus considered as an ideal information carrier for next generation spintronic devices [6–12]. Skyrmion transport behavior at room temperature, either the thermal activated diffusion or the directional drift under an external field applied [13,14], is one of the key issues for the application of skyrmion-based functional devices [15–18] and attracts considerable attention [19–22]. Micromagnetic simulations found the skyrmion diffusion in a defect-free system does not exert a migratory barrier at finite temperatures [13,14]. However, recent experiments [17,23] observed the Arrhenius diffusion behavior, which reveals the presence of a migration barrier for skyrmion transport. Subsequent theoretical studies suggested that it is speculated to be the pinning effects induced by the crystalline defects [17,23,24]. Although this is accepted to be a reasonable interpretation, the underlying microdynamic mechanism is still unclear. In magnetic materials, spins attach to the atomic lattices, naturally leading to the intrinsic spin-lattice coupling, so that the local skyrmion spin texture is found to accompany a local lattice distortion field [25,26] [LLDF, see in Figs. 1(a) and 1(b)], and the latter can undoubtedly return the influence to the spin-spin interaction [27] and the resulting microdynamic evolution of a skyrmion [25–30]. Therefore, it is necessary to clarify the influence of the LLDF on the skyrmion transport, which is the aim of this current Letter.

Before introducing the microdynamics, let us discuss the general evolution behavior of a skyrmion first. For the sake of generality, a single skyrmion in an isotropic thin film is considered here. Treated as a Brownian particle, the in-plane (e.g., xy plane) evolution of the skyrmion is described by a stochastic Thiele equation [13,20,31]

$$m\dot{\boldsymbol{v}} = \boldsymbol{F}(\boldsymbol{r}) + \boldsymbol{G}\times\boldsymbol{v} - \Gamma\boldsymbol{v} + \boldsymbol{\eta}(t). \tag{1}$$

Here, m, $\boldsymbol{v}$, and $\boldsymbol{r}$ are the effective mass, velocity and position of the skyrmion, respectively. The conservative force $\boldsymbol{F} = -\boldsymbol{\nabla}U + \boldsymbol{F}_{\mathrm{ext}}$ acting on the skyrmion is made up of the migration potential barrier $-\boldsymbol{\nabla}U$ and an applied external force $\boldsymbol{F}_{\mathrm{ext}}$. The term $\boldsymbol{G}\times\boldsymbol{v}$ is the Magnus force, with $\boldsymbol{G} = G\hat{\boldsymbol{z}}$ as the gyromagnetic vector. The terms $-\Gamma\boldsymbol{v}$ and $\boldsymbol{\eta}(t)$ are the frictional and random forces, respectively, denoting the dissipation and fluctuation actions arising from the thermal vibrations of spins, with Γ as the dissipative coefficient. The physical mechanism of Eq. (1) is to treat a skyrmion as a "particle" embedded in a noise environment [in terms of $-\Gamma\boldsymbol{v} + \boldsymbol{\eta}(t)$] and the conservative force field $\boldsymbol{F}$ [13,20]. Accordingly, without the migration barrier, i.e., $U = 0$, the skyrmion transport is a nondirectional free Brownian motion when $\boldsymbol{F}_{\mathrm{ext}} = 0$, where the diffusivity depends on temperature linearly as $D = \mu_d k_B T$, with $\mu_d = \Gamma/[G^2 + \Gamma^2]$ as the mobility [13,14]; otherwise, skyrmion transport is a directional diffusion when applying an $\boldsymbol{F}_{\mathrm{ext}}$, like electric current [7,32] and magnetic field gradient [33,34], where the terminal velocity $\boldsymbol{v}_d$ at the steady state is proportional to $\boldsymbol{F}_{\mathrm{ext}}$ [35].

In fact, Eq. (1) is equivalent to the Langevin equation for the stochastic motion of a Brownian particle embedded in a noisy environment and the conservative potential field. Based on Kramer's theory [36], issues about the

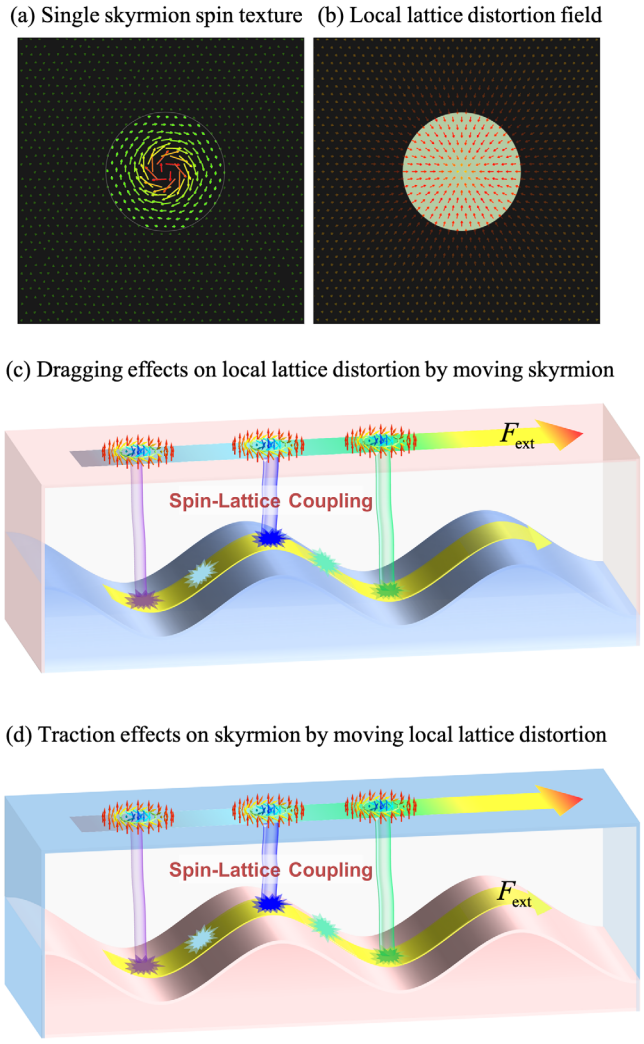

FIG. 1. The schematics of (a) a single skyrmion spin texture and (b) the corresponding LLDF $\varepsilon(\boldsymbol{r})$ defined in Eq. (5). In (a), the arrows denote the in-plane atomic spin vectors $\boldsymbol{S}_i$, colored by their out-of-plane projections. In (b), the arrows denote the atomic displacements with respect to their lattice sites. (c) and (d) demonstrate the effects of the LLDF: (i) when the skyrmion moves along its track by $\boldsymbol{F}_{\text{ext}}$, the LLDF provides a dragging force on the skyrmion shown in (c); (ii) when the LLDF is forced to move by $\boldsymbol{F}_{\text{ext}}$, the skyrmion exerts an traction force shown in (d), which drives it to keep up with the LLDF. In (c) and (d), the colored arrows represent a skyrmion texture on top; the colored sparks denote the LLDF upon its conservative potential field having the same crystalline periodicity as the host crystal; and the colored rods connecting between the skyrmion and the LLDF represent their interactions due to the spin-lattice coupling effects.

Brownian particle escaping the migration barrier have been thoroughly studied. Substantial progress has been made on the underlying mechanistic understanding of these stochastic behaviors using a similar methodology in many other related areas, such as the solute diffusion in metals [37,38] and the polarization relaxation in ferroelectrics [39]. For example, the solute diffusion without applying $\boldsymbol{F}_{\text{ext}}$ reveals a typical low energy activation behavior [40], relying on the competition between the migration energy E_m and the thermal energy k_BT: (1) the diffusivity obeys Arrhenius law when $E_m \gg k_BT$ as $D/D_0 = \exp(-E_m/k_BT)$; (2) effects of migration potential is negligible when $E_m \ll k_BT$, so that the diffusion is of Einstein type as $D = \mu_d k_BT$; (3) in the intermediate temperature region, the Brownian particle reveals a mixed diffusion behavior.

In analogy to solute diffusion, the skyrmion transport described by Eq. (1) is expected to be significantly affected by the presence of a migration barrier. Note that the solute diffusion is implemented as random hops between its equilibrium sites, so that the migration barrier for the whole transport process naturally has a similar crystalline periodicity as that of the host crystal, leading to a well-defined Arrhenius behavior when $E_m \gg k_BT$. In the case of skyrmion diffusion, the crystalline defects are speculated to be responsible for the migration barrier [41–44]. However, since the defects usually move too slowly to keep up with the skyrmion transport when $E_m \gg k_BT$ and the resulting migration barrier is determined by the distribution of defects, the skyrmion hops only between the defects' locations [45]. In this case, the skyrmion indicates Arrhenius behavior near the region filled by defects, but Einstein behavior in the defect-free region, so to reveal a complicated non-Arrhenius behavior. In our opinion, the pinning effects from crystalline defects might not be the most probable reason for the Arrhenius behavior of skyrmions observed in experiments, and another possibility should be considered.

In the following, we will perform atomistic spin-lattice dynamics (SLD) simulations [26] to study the effects of the LLDF. As schematics in Fig. 1, the LLDF, which exerts a conservative potential field having the same crystalline periodicity as the host crystal, is another source of migration barrier leading to the similar transport behavior of a skyrmion as the solute diffusion in metals: (i) when the skyrmion moves along its track under $\boldsymbol{F}_{\text{ext}}$, the LLDF provides a dragging force on the skyrmion through spin-lattice coupling; (ii) when the LLDF is forced to move by $\boldsymbol{F}_{\text{ext}}$, it will provide a traction force on the skyrmion, which drives the skyrmion to keep up with the LLDF.

In SLD, the defect-free skyrmion system is treated as an ensemble of N interactive atoms with spin and lattice degrees of freedom, whose microdynamics is described by the Hamiltonian $\mathcal{H}_{S+L}$ as

$$\mathcal{H}_{S+L} = \mathcal{H}_L + \mathcal{H}_S. \tag{2}$$

Here, $\mathcal{H}_L$ describes the nonmagnetic lattice dynamics,

$$\mathcal{H}_L = \sum_{i=1}^{N} \frac{\boldsymbol{p}_i^2}{2m_i} + U(\{\boldsymbol{r}_i\}), \tag{3}$$

where m_i, $\boldsymbol{p}_i$, and $\boldsymbol{r}_i$ are the atomic mass, momentum, and position of the ith atom, respectively, and $U(\{\boldsymbol{r}_i\})$ describes the nonmagnetic interatomic interactions. $\mathcal{H}_S$ describes the spin-spin interactions, including the Heisenberg exchange interaction (HEI), Dzyaloshinsky-Moriya interaction (DMI), and Zeeman interaction (ZI), as

$$\mathcal{H}_S = -\sum_{i>j}[J_{ij}(\boldsymbol{r})\boldsymbol{S}_i\cdot\boldsymbol{S}_j + \boldsymbol{D}_{ij}(\boldsymbol{r})\cdot(\boldsymbol{S}_i\times\boldsymbol{S}_j)] - \sum_i \boldsymbol{H}_{\text{ext}}\cdot\boldsymbol{S}_i. \quad (4)$$

Here, $\boldsymbol{S}_i$ denotes the ith atomic spin, and $\boldsymbol{H}_{\text{ext}}$ is the applied magnetic field. $J_{ij}(\boldsymbol{r})$ and $\boldsymbol{D}_{ij}(\boldsymbol{r})$ are the strengths of HEI and DMI, respectively, relying on the instantaneous lattice configuration $\boldsymbol{r} \equiv \{\boldsymbol{r}_i\}$, giving rise to the intrinsic spin-lattice coupling. In other words, the form and amplitude of $J_{ij}(\boldsymbol{r})$ and $\boldsymbol{D}_{ij}(\boldsymbol{r})$ are the atomistic representation of the intrinsic spin-lattice coupling, which affects the size and amplitude of the LLDF and the parameters characterizing skyrmion transport behavior. The synergistic effects of HEI, DMI, and ZI result in the skyrmion spin texture [26]. Because of the spin-lattice coupling, the local spiral spin texture of the skyrmion is found to be accompanied with a LLDF [25,26] as shown in Fig. 1(b). The LLDF $\varepsilon(\boldsymbol{r}_i)$ is defined as

$$\varepsilon(\boldsymbol{r}_i) = (\boldsymbol{r}_i - \boldsymbol{r}_i^0)/a \quad (5)$$

where $\boldsymbol{r}_i^0$ is the ith lattice site of a perfect crystal, and a is the lattice constant. To study the spin-lattice coupling effects, a pure spin dynamics system governed by $\mathcal{H}_S$ is designed as a reference, where the lattice dynamics is shut down, and the spin dynamics is attached to the given fixed lattice configuration. In fact, the spin dynamics governed by $\mathcal{H}_S$ is the same as that in a micromagnetic model [14]. In this regard, comparing simulation results based on $\mathcal{H}_{S+L}$ and $\mathcal{H}_S$, we can analyze the influence of the LLDF on skyrmion transport behavior. To discuss the underlying mechanism, all the values of physical quantities in our simulations are normalized to the corresponding characteristic ones, as widely implemented in other simulations [46] (see simulation details in the Supplemental Material [47]).

When $\boldsymbol{F}_{\text{ext}} = 0$, the free Brownian motion of the skyrmion is observed in a defect-free system. Figure 2(a) plots the temperature dependence of skyrmion diffusivity $D = D(T)$ with ($\mathcal{H}_{S+L}$) and without ($\mathcal{H}_S$) spin-lattice coupling, respectively. For $\mathcal{H}_S$, since there is no LLDF offering the migration barrier in the defect-free system, the skyrmion diffusivity follows Einstein theory as $D = \mu_d k_B T$ with $\mu_d = 2.15 \times 10^{-3}[a^2/\hbar]$, which is consistent with the predictions of micromagnetic simulations [14]. For $\mathcal{H}_{S+L}$, the skyrmion reveals the similar non-Arrhenius behavior with the solute diffusion affected by a migration barrier. In particular, the typical Arrhenius behavior is revealed

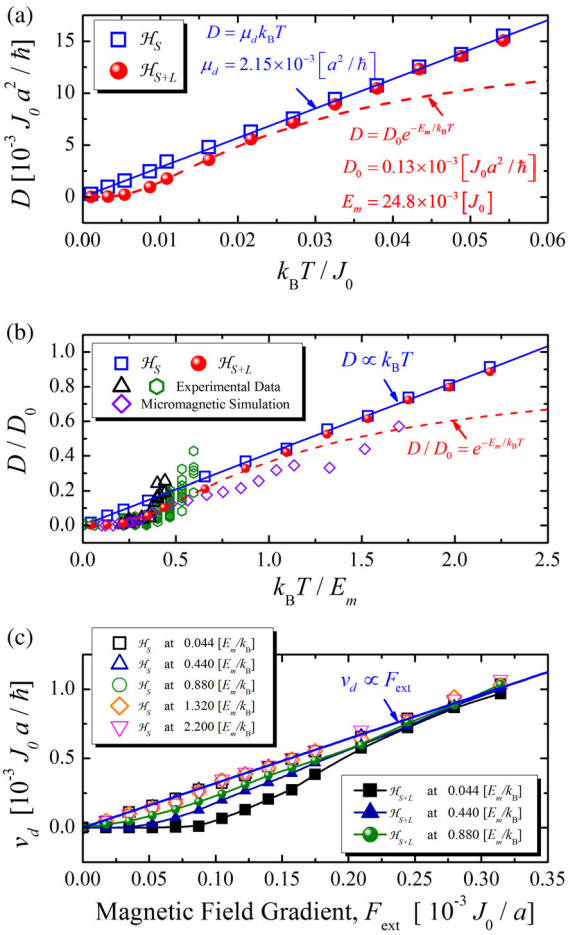

FIG. 2. The SLD simulation of a single skyrmion Brownian motion. (a) The diffusivity D is plotted as a function of temperature in terms of $k_B T/J_0$ without the external force applied. (b) The reconstructed simulation data of D in accordance with Arrhenius law as $D/D_0 = e^{-E_m/k_B T}$, as well as data in other studies. (c) The terminal velocity v_d is plotted as a function of applied magnetic field gradient F_{ext}.

for skyrmion diffusion, as $D = D_0 \exp(-E_m/k_B T)$ at $k_B T/J_0 < 0.02$ with $D_0 = 0.13 \times 10^{-3}[J_0 a^2/\hbar]$ and $E_m = 24.8 \times 10^{-3}[J_0]$ shown in Fig. 2(a), which is consistent with the experimental measurements [17,23] and micromagnetic simulation [14]. In Fig. 2(b), we reconstruct the skyrmion diffusion data obtained from $\mathcal{H}_{S+L}$, and the simulations [14] and experiments [17,23] from other studies in accordant with Arrhenius law of $D/D_0 = e^{-E_m/k_B T}$. Here D_0 and E_m are the fitting parameters, which are associated with the physical properties of materials (see details in the Supplemental Material [47]). It is found that the skyrmion diffusivity well obeys the Arrhenius law at low temperatures (e.g., $k_B T/E_m < 0.5$). When the temperature increases up to $k_B T/E_m > 1.0$, the LLDF influence in $\mathcal{H}_{S+L}$ is negligible, so that the skyrmion diffusivity is the as same as that in $\mathcal{H}_S$. Therefore, the simulation results based on $\mathcal{H}_{S+L}$ demonstrate the existence of a migration barrier for skyrmion diffusion without any $\boldsymbol{F}_{\text{ext}}$ applied.

Furthermore, the effects of a migration barrier can also be found in the case of the driven transport of a skyrmion by applying the external magnetic field gradient F_{ext}. Without the LLDF in $\mathcal{H}_S$, any F_{ext} applied can result in the directional drift of a skyrmion and $v_d \propto F_{\mathrm{ext}}$ at all the temperatures considered in Fig. 2(c), which is consistent with other simulations [33,34]. However, for $\mathcal{H}_{S+L}$, because of the presence of migration barrier, the small F_{ext}, e.g., $F_{\mathrm{ext}} < 0.07 \times 10^{-3}[J_0/a]$, cannot lead to a significant directional drift of a skyrmion at low temperatures, e.g., $k_BT/E_m = 0.044$. Although the migration barrier is suppressed by small F_{ext}, the thermal energy of the skyrmion gained from spin dynamics is too weak to let it escape the barrier [45]. Otherwise, increasing F_{ext} leads to more significant driven transport, e.g., when $F_{\mathrm{ext}} > 0.25 \times 10^{-3}[J_0/a]$, the barrier is suppressed to be negligible, so that the skyrmion reveals the same Einstein behavior as that in $\mathcal{H}_S$. Similar transport phenomena were also reported in the case of a skyrmion driven by applying electric current [35,59]. On the other hand, increasing temperatures can also enhance the driven transport of a skyrmion. Plotted in Fig. 2(c), as k_BT/E_m increasing from 0.044 up to 0.88, the critical value of F_{ext} to ignite the observable directional drift reduces significantly from $\sim 0.07 \times 10^{-3}[J_0/a]$ to zero.

From the simulation results of $\mathcal{H}_{S+L}$, both the free diffusion and the directional drift under an applied magnetic field gradient, the skyrmion transport is significantly affected by the spontaneous LLDF arising from the spin-lattice coupling effects, which is associated with the migration energy barrier for the skyrmion transport, and the diffusion behavior is well consistent with the physical picture of the solute diffusion in metals [37,38].

To further verify the above conjecture, we artificially design an ideal LLDF, and detect the skyrmion transport behavior through the pure spin dynamics governed by $\mathcal{H}_S$ (see detail in the Supplemental Material [47]). At the initial moment of the simulation, an ideal LLDF is constructed at the position coinciding with the skyrmion center. This LLDF then moves artificially along the x direction, which drags the skyrmion because of the spin-lattice coupling. Under the synergistic effects of the Magnus force [60] and the traction of the LLDF, the skyrmion experiences a transport process with gyromotion [23,61]. When the LLDF stops moving, the skyrmion rotates around the LLDF until the energy is dissipated and is finally pinned near the LLDF as demonstrated in Fig. 3.

In addition, Fig. 4(a) indicates the energy dissipation process of the system for skyrmion traction movement, which is a typical relaxation process [39]. The mean time τ required by the skyrmion traction movement from the old site to the new location of the LLDF is estimated as $\tau \sim 50[\hbar/J_0]$, which is smaller than the mean diffusion time

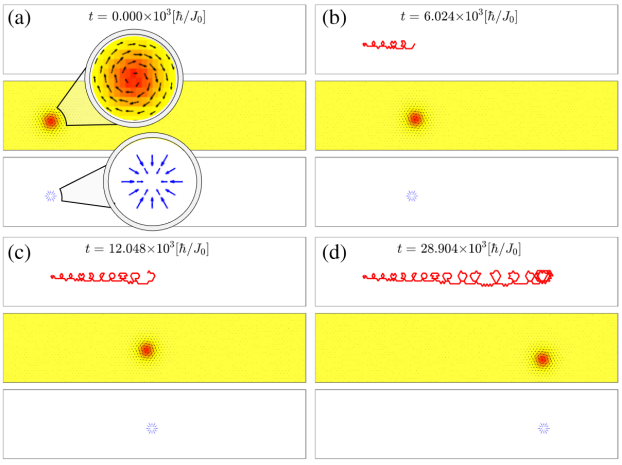

FIG. 3. Snapshots of traction movement of the skyrmion by the movement of an ideal LLDF, (a) $t = 0$, (b) $t = 6.024 \times 10^3[\hbar/J_0]$, (c) $t = 12.048 \times 10^3[\hbar/J_0]$, and (d) $t = 28.904 \times 10^3[\hbar/J_0]$. In each subfigure, the in-plane skyrmion trajectory is presented on top; spin configuration in the middle; the blue arrows demonstrate a designed ideal LLDF, given in the bottom. The online movies are provided and show the detailed evolution process.

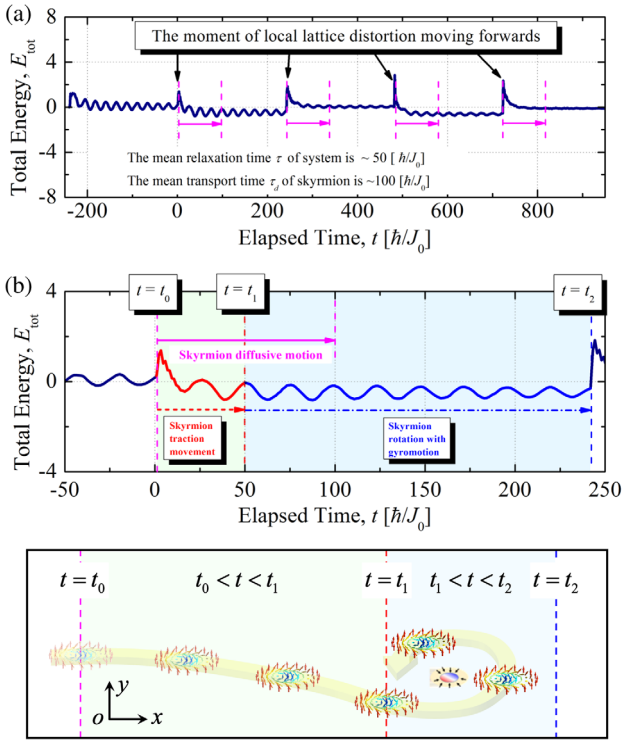

FIG. 4. (a) The energy dissipation with the skyrmion traction movement. The time interval within two dashed lines indicates the mean duration for skyrmion diffusion, $\tau_d \sim 100[\hbar/J_0]$. (b) The skyrmion motion in the first period. Here, after suddenly moving the ideal LLDF to a new position at $t = t_0 = 0$, the skyrmion traction movement occurs in the duration of $t_0 < t < t_1$ with $t_1 \sim 50[\hbar/J_0]$, then it rotates around with gyromotion until the next move of the LLDF at $t = t_2 \sim 240[\hbar/J_0]$. Reader can see the online movie for the detailed process.

of the skyrmion τ_d estimated from Fig. 2, as $\tau_d \sim 100[\hbar/J_0]$ (see detail in Supplemental Materials [47]). Figure 4(b) gives the detailed information for a single traction step: after the artificial move of the ideal LLDF at $t = t_0 = 0$, the skyrmion traction movement occurs in $t = t_1 \sim 50[\hbar/J_0]$; then the skyrmion rotates around the new position of the LLDF with gyromotion until the next move of the LLDF occurs at $t = t_2 \sim 240[\hbar/J_0]$. Therefore, the LLDF can keep up with the skyrmion diffusion, and provides the migration barrier to the transport behavior.

Note that the spin-lattice coupling effects are implemented by the lattice dependence of both $J_{ij}(\boldsymbol{r})$ and $\boldsymbol{D}_{ij}(\boldsymbol{r})$ by a simplified functional form in the current work (see Sec. S2 of the Supplemental Material [47]). In principle, the functional form and amplitude of $J_{ij}(\boldsymbol{r})$ and $\boldsymbol{D}_{ij}(\boldsymbol{r})$ should be fitted from electronic scale *ab initio* calculations [62,63]. However, on the basis of such a simplification treatment for the spin-lattice coupling, the interactions between the LLDF and the skyrmion spin texture are reproduced, giving rise to the non-Arrhenius behavior of the skyrmion transport. In addition, we further discuss the influence of the different form and amplitude of $J_{ij}(\boldsymbol{r})$ and $\boldsymbol{D}_{ij}(\boldsymbol{r})$ to the LLDF and skyrmion transport (see detail in Sec. S6 of Supplemental Materials [47]). It is found that varying the form and amplitude of $J_{ij}(\boldsymbol{r})$ and $\boldsymbol{D}_{ij}(\boldsymbol{r})$ leads to the variation of the LLDF size and distribution, and the transport behavior of the skyrmion is still of the non-Arrhenius type, because of the presence of the LLDF and the resulting interaction between the LLDF and the skyrmion.

In summary, we perform atomistic SLD simulations to study the spin-lattice coupling effects on skyrmion transport in a defect-free system. The resulting spontaneous LLDF is affirmed to provide an migration barrier for the skyrmion transport and the complicated non-Arrhenius behavior, which is consistent with the physical picture of the solution diffusion. Through an artificially designed simulation, the relationship between the skyrmion and the LLDF is further verified. Our results also agree with other simulations and experimental measurements. It can be expected that the spin-lattice coupling effects have great potential for precisely controlling the skyrmion and designing related skyrmion-based spintronic devices.

We thank our colleagues in SYSU, including Wenpeng Zhu, Xin Luo, Jianyi Liu, Long Zhu, and Kan Lai, for helpful discussion and valuable comments on the manuscript. This work was supported by the National Natural Science Foundation of China (NSFC) (Grants No. 12072379, No. 11904415, and No. 11972382). by the National Natural Science Foundation of Guangdong Province, China (Grants No. 2021A1515010346, and No. 2021A1515010348). The simulations reported were performed on resources provided by the National Supercomputer Center in Guangzhou.

*Corresponding author.
wenhh3@mail.sysu.edu.cn
†Corresponding author.
zhengy35@mail.sysu.edu.cn

[1] S. Mühlbauer, B. Binz, F. Jonietz, C. Pfleiderer, A. Rosch, A. Neubauer, R. Georgii, and P. Böni, Science **323**, 915 (2009).
[2] X. Yu, Y. Onose, N. Kanazawa, J. Park, J. Han, Y. Matsui, N. Nagaosa, and Y. Tokura, Nature (London) **465**, 901 (2010).
[3] N. Romming, C. Hanneken, M. Menzel, J. E. Bickel, B. Wolter, K. von Bergmann, A. Kubetzka, and R. Wiesendanger, Science **341**, 636 (2013).
[4] N. Nagaosa and Y. Tokura, Nat. Nanotechnol. **8**, 899 (2013).
[5] S. Woo, K. Litzius, B. Krüger, M.-Y. Im, L. Caretta, K. Richter, M. Mann, A. Krone, R. M. Reeve, M. Weigand *et al.*, Nat. Mater. **15**, 501 (2016).
[6] A. Fert, V. Cros, and J. Sampaio, Nat. Nanotechnol. **8**, 152 (2013).
[7] J. Sampaio, V. Cros, S. Rohart, A. Thiaville, and A. Fert, Nat. Nanotechnol. **8**, 839 (2013).
[8] X. Zhang, M. Ezawa, and Y. Zhou, Sci. Rep. **5**, 9400 (2015).
[9] R. Wiesendanger, Nat. Rev. Mater. **1**, 16044 (2016).
[10] Y. Zheng and W. J. Chen, Rep. Prog. Phys. **80**, 086501 (2017).
[11] A. Fert, N. Reyren, and V. Cros, Nat. Rev. Mater. **2**, 17031 (2017).
[12] G. Yu, P. Upadhyaya, Q. Shao, H. Wu, G. Yin, X. Li, C. He, W. Jiang, X. Han, P. K. Amiri *et al.*, Nano Lett. **17**, 261 (2017).
[13] C. Schütte, J. Iwasaki, A. Rosch, and N. Nagaosa, Phys. Rev. B **90**, 174434 (2014).
[14] J. Miltat, S. Rohart, and A. Thiaville, Phys. Rev. B **97**, 214426 (2018).
[15] Y. Huang, W. Kang, X. Zhang, Y. Zhou, and W. Zhao, Nanotechnology **28**, 08LT02 (2017).
[16] D. Pinna, F. Abreu Araujo, J.-V. Kim, V. Cros, D. Querlioz, P. Bessiere, J. Droulez, and J. Grollier, Phys. Rev. Applied **9**, 064018 (2018).
[17] J. Zázvorka, F. Jakobs, D. Heinze, N. Keil, S. Kromin, S. Jaiswal, K. Litzius, G. Jakob, P. Virnau, D. Pinna *et al.*, Nat. Nanotechnol. **14**, 658 (2019).
[18] Y. Jibiki, M. Goto, E. Tamura, J. Cho, S. Miki, R. Ishikawa, H. Nomura, T. Srivastava, W. Lim, S. Auffret *et al.*, Appl. Phys. Lett. **117**, 082402 (2020).
[19] S.-Z. Lin, C. Reichhardt, C. D. Batista, and A. Saxena, Phys. Rev. B **87**, 214419 (2013).
[20] R. E. Troncoso and Á. S. Núñez, Ann. Phys. (Amsterdam) **351**, 850 (2014).
[21] C. Reichhardt and C. Reichhardt, J. Phys. Condens. Matter **31**, 07LT01 (2019).
[22] M. Mochizuki, X. Yu, S. Seki, N. Kanazawa, W. Koshibae, J. Zang, M. Mostovoy, Y. Tokura, and N. Nagaosa, Nat. Mater. **13**, 241 (2014).
[23] L. Zhao, Z. Wang, X. Zhang, X. Liang, J. Xia, K. Wu, H.-A. Zhou, Y. Dong, G. Yu, K. L. Wang *et al.*, Phys. Rev. Lett. **125**, 027206 (2020).
[24] T. Nozaki, Y. Jibiki, M. Goto, E. Tamura, T. Nozaki, H. Kubota, A. Fukushima, S. Yuasa, and Y. Suzuki, Appl. Phys. Lett. **114**, 012402 (2019).

[25] Y. Shi and J. Wang, Phys. Rev. B **97**, 224428 (2018).
[26] Y. Wu, H. Wen, J. Liu, K. Lai, and Y. Zheng, Phys. Rev. B **100**, 144310 (2019).
[27] D. A. Kitchaev, I. J. Beyerlein, and A. Van der Ven, Phys. Rev. B **98**, 214414 (2018).
[28] K. Shibata, J. Iwasaki, N. Kanazawa, S. Aizawa, T. Tanigaki, M. Shirai, T. Nakajima, M. Kubota, M. Kawasaki, H. Park *et al.*, Nat. Nanotechnol. **10**, 589 (2015).
[29] J.-M. Hu, T. Yang, and L.-Q. Chen, Acta Mater. **183**, 145 (2020).
[30] J.-M. Hu, T. Yang, and L.-Q. Chen, npj Comput. Mater. **4**, 62 (2018).
[31] A. Thiele, Phys. Rev. Lett. **30**, 230 (1973).
[32] J. Iwasaki, M. Mochizuki, and N. Nagaosa, Nat. Commun. **4**, 1463 (2013).
[33] C. Wang, D. Xiao, X. Chen, Y. Zhou, and Y. Liu, New J. Phys. **19**, 083008 (2017).
[34] J. Liang, J. Yu, J. Chen, M. Qin, M. Zeng, X. Lu, X. Gao, and J.-M. Liu, New J. Phys. **20**, 053037 (2018).
[35] R. E. Troncoso and A. S. Núñez, Phys. Rev. B **89**, 224403 (2014).
[36] H. A. Kramers, Physica **7**, 284 (1940).
[37] H. Wen, A. A. Semenov, and C. H. Woo, J. Nucl. Mater. **493**, 21 (2017).
[38] K. Lai, H. Wen, J. Liu, Y. Wu, and Y. Zheng, J. Nucl. Mater. **524**, 286 (2019).
[39] J. Liu, H. Wen, W. Chen, and Y. Zheng, Phys. Rev. B **103**, 014308 (2021).
[40] G. Henkelman, Annu. Rev. Mater. Res. **47**, 199 (2017).
[41] C. Reichhardt, D. Ray, and C. J. Olson Reichhardt, Phys. Rev. Lett. **114**, 217202 (2015).
[42] J. Müller and A. Rosch, Phys. Rev. B **91**, 054410 (2015).
[43] Y.-H. Liu and Y.-Q. Li, J. Phys. Condens. Matter **25**, 076005 (2013).
[44] J.-V. Kim and M.-W. Yoo, Appl. Phys. Lett. **110**, 132404 (2017).
[45] C. Reichhardt and C. J. O. Reichhardt, Rep. Prog. Phys. **80**, 026501 (2017).
[46] W. Wang, M. Beg, B. Zhang, W. Kuch, and H. Fangohr, Phys. Rev. B **92**, 020403(R) (2015).
[47] See Supplemental Material at http://link.aps.org/supplemental/10.1103/PhysRevLett.127.097201 for values of the characteristic quantities used to normalize the one in main context (Sec. S1); sinulation detail of spin-lattice dynamics, which includes Refs. [48–53] (Sec. S2); calculation of skyrmion diffusion without external field (Sec. S3); calculation of skyrmion directional drift under an external field (Sec. S4); the traction of local lattice distortion on skyrmion (Sec. S5), and effects of functional form of $J_{ij}(r)$ and $D_{ij}(r)$ on skyrmion transport (Sec. S6), which includes Refs. [54–58].
[48] P.-W. Ma, C. H. Woo, and S. L. Dudarev, Phys. Rev. B **78**, 024434 (2008).
[49] C. Feng, F. Meng, Y. Wang, J. Jiang, N. Mehmood, Y. Cao, X. Lv, F. Yang, L. Wang, Y. Zhao, S. Xie, Z. Hou, W. Mi, Y. Peng, K. Wang, X. Gao, G. Yu, and J. Liu, Adv. Funct. Mater. **31**, 2008715 (2021).
[50] J. Chen, W. P. Cai, M. H. Qin, S. Dong, X. B. Lu, X. S. Gao, and J.-M. Liu, Sci. Rep. **7**, 7392 (2017).
[51] Y. Nii, A. Kikkawa, Y. Taguchi, Y. Tokura, and Y. Iwasa, Phys. Rev. Lett. **113**, 267203 (2014).
[52] N. Hatano and M. Suzuki, Finding exponential product formulas of higher orders, in *Quantum Annealing and Other Optimization Methods*, edited by A. Das and B. K. Chakrabarti (Springer Berlin Heidelberg, Berlin, Heidelberg, 2005), pp. 37–68.
[53] P.-W. Ma and C. H. Woo, Phys. Rev. E **79**, 046703 (2009).
[54] A. Y. Deviatov, I. A. Iakovlev, and V. V. Mazurenko, Phys. Rev. Applied **12**, 054026 (2019).
[55] C. Psaroudaki and D. Loss, Phys. Rev. Lett. **120**, 237203 (2018).
[56] T. Koretsune, N. Nagaosa, and R. Arita, Sci. Rep. **5**, 13302 (2015).
[57] J. Hagemeister, E. Y. Vedmedenko, and R. Wiesendanger, Phys. Rev. B **94**, 104434 (2016).
[58] H. Yang, A. Thiaville, S. Rohart, A. Fert, and M. Chshiev, Phys. Rev. Lett. **115**, 267210 (2015).
[59] T. Schulz, R. Ritz, A. Bauer, M. Halder, M. Wagner, C. Franz, C. Pfleiderer, K. Everschor, M. Garst, and A. Rosch, Nat. Phys. **8**, 301 (2012).
[60] F. Jonietz, S. Mühlbauer, C. Pfleiderer, A. Neubauer, W. Münzer, A. Bauer, T. Adams, R. Georgii, P. Böni, R. A. Duine *et al.*, Science **330**, 1648 (2010).
[61] W. Chen, L. Liu, Y. Ji, and Y. Zheng, Phys. Rev. B **99**, 064431 (2019).
[62] H. Wang, P.-W. Ma, and C. H. Woo, Phys. Rev. B **82**, 144304 (2010).
[63] H. Ebert, D. Koedderitzsch, and J. Minar, Rep. Prog. Phys. **74**, 096501 (2011).